Journal of Rock Mechanics and Geotechnical Engineering 15 (2023) 1052–1064

Contents lists available at ScienceDirect

Journal of Rock Mechanics and Geotechnical Engineering

journal homepage: www.jrmge.cn

Technical Note

Multivariate adaptive regression splines analysis for 3D slope stability in anisotropic and heterogenous clay

Jim Shiau [a], Van Qui Lai [b,c,*], Suraparb Keawsawasvong [d]

[a] School of Civil Engineering and Surveying, University of Southern Queensland, Toowoomba, Queensland, 4350, Australia
[b] Faculty of Civil Engineering, Ho Chi Minh City University of Technology (HCMUT), 268 Ly Thuong Kiet Street, District 10, Ho Chi Minh City, Viet Nam
[c] Vietnam National University Ho Chi Minh City (VNU-HCM), Linh Trung Ward, Thu Duc District, Ho Chi Minh City, Viet Nam
[d] Department of Civil Engineering, Thammasat School of Engineering, Thammasat University, Pathumthani, Bangkok, 12120, Thailand

ARTICLE INFO

Article history:
Received 27 February 2022
Received in revised form
3 May 2022
Accepted 15 May 2022
Available online 30 June 2022

Keywords:
3D undrained slope
Limit analysis
Anisotropy
Heterogeneity

ABSTRACT

Little research can be found in relation to the stability of anisotropic and heterogenous soils in three dimensions. In this paper, we propose a study on the three-dimensional (3D) undrained slopes in anisotropic and heterogenous clay using advanced upper and lower bounds finite element limit analysis (FELA). The obtained stability solutions are normalized, and presented by a stability number that is a function of three geometrical ratios and two material ratios, i.e. depth ratio, length ratio, slope angle, shear strength gradient ratio and anisotropic strength ratio. Numerical results are compared with experimental data in the literature, and charts are presented to cover a wide range of design parameters. Using the multivariate adaptive regression splines (MARS) analysis, the respective influence and sensitivity of each design parameter on the stability number and the failure mechanism are investigated. An empirical equation is also developed to effectively estimate the stability number.

1. Introduction

Assessing the stability of slopes is commonly required in construction projects. The slope stability research has drawn great attention since 1930s (Taylor, 1937, 1948; Bishop, 1955; Morgenstern and Price, 1965; Janbu, 1973; Leshchinsky and Baker, 1986; Leshchinsky and Huang, 1992; Chang, 2002; Shiau et al., 2008a, b, 2011; Li et al., 2009; Xie et al., 2011; Zhang et al., 2012; Ukritchon and Keawsawasvong, 2018; Renani and Martin, 2020; Yang et al., 2020). In general, the stability of a slope is largely influenced by the geometry of the slope and the physical properties of soils. The assessment of slope stability is normally expressed by a stability number using slope stability charts (Taylor, 1937). The research into slope stability has been further extended to three dimensions (Shiau and Watson, 2008; Li et al., 2009, 2014b; Lu, 2015; Qian et al., 2015; Ma et al., 2021; Yang and Chen, 2021; Zhang and Yang, 2021). Several researchers, such as Baligh and Azzouz (1975), Azzouz and Baligh (1978), and Gens et al. (1988), have pointed out that two-dimensional (2D) slope analysis which neglects the three-dimensional (3D) effects may lead to an underestimate of the factor of safety.

In the past few decades, the computational methods for the stability analysis of 3D slopes have been developed, including the limit equilibrium method (LEM), finite element method (FEM), and finite element limit analysis (FELA) method. Although LEM is the most commonly-used one (Morgenstern and Price, 1965; Li et al., 2014b; Schlotfeldt et al., 2018; Siacara et al., 2020; Ardestani et al., 2021), it requires an initial assumption of the slip surface (Kainthola et al., 2013; Azarafza et al., 2021). The FEM outperforms LEM in predicting 3D slope stability without the need of assuming the potential slip surface (Griffiths and Lane, 1999; Griffiths and Marquez, 2007; Guo et al., 2011; Chai et al., 2013; Yang et al., 2015; Raghuvanshi, 2019; Ghadrdan et al., 2021). Nevertheless, due to the excessive requirement of computational time, it has not been widely used to produce 3D slope stability charts. The recently developed FELA, such as lower bound (LB) and upper bound (UB) limit analysis using nonlinear programming and finite elements have become popular in studying 3D slope owing to its computational efficiency (Loukidis et al., 2003; Kumar and Samui, 2006; Li et al., 2009, 2014a; Kardani et al., 2021).

* Corresponding author. Faculty of Civil Engineering, Ho Chi Minh City University of Technology (HCMUT), 268 Ly Thuong Kiet Street, District 10, Ho Chi Minh City, Viet Nam.
E-mail address: lvqui@hcmut.edu.vn (V.Q. Lai).

Peer review under responsibility of Institute of Rock and Soil Mechanics, Chinese Academy of Sciences.

https://doi.org/10.1016/j.jrmge.2022.05.016

Apart from the 3D analysis, many studies have discovered that the anisotropic behavior of natural clays can affect the stability performance of soil structures (e.g. Casagrande and Carillo, 1944; Lo, 1965; Ladd, 1991; Ladd and DeGroot, 2003; Ukritchon and Keawsawasvong, 2019a, b, 2020a, b; Keawsawasvong and Ukritchon, 2021, 2022). Recently, Krabbenhoft et al. (2019) proposed an anisotropic undrained shear (AUS) model that can be used to study the behavior of anisotropic clays by adopting the generalized Tresca (GT) failure criterion (Krabbenhoft and Lyamin, 2015). The AUS model has recently been implemented in the 3D FELA software, OptumG3 (OptumCE, 2020), and it has been successfully applied to solving many geotechnical stability problems (Keawsawasvong et al., 2021, 2022a; Nguyen et al., 2021; Yodsomjai et al., 2021a; Jearsiripongkul et al., 2022; Lai et al., 2022a, b; Sirimontree et al., 2022). Note that FELA has been used by several researchers in the past (e.g. Shiau et al., 2004, 2006, 2011; Ukritchon and Keawsawasvong, 2017, 2019c, d; Keawsawasvong and Ukritchon, 2019a, b, 2020; Ukritchon et al., 2019, 2020; Shiau and Al-Asadi, 2020a, b, 2021a, b, 2022; Yodsomjai et al., 2021b; Keawsawasvong and Shiau, 2022; Shiau et al., 2022). Nevertheless, it has not been rigorously assessed using the new technique with LB and UB solutions considering both anisotropic and heterogenous effects.

Following the work of Keawsawasvong et al. (2022a), this paper aims to present novel stability solutions of 3D undrained slopes in anisotropic and heterogenous clay using rigorous LB and UB FELA and AUS failure criterion. The 3D stability solutions of averaged LB and UB are formulated by a dimensionless stability number that is a function of five dimensionless input parameters: depth ratio, length ratio, slope angle, shear strength gradient ratio, and anisotropic strength ratio. The associated failure mechanism of each parametric effect is also investigated so that the fundamental influence of all dimensionless input parameters can be demonstrated. Due to the complexity of the problem with five dimensionless parameters, it is important to determine the sensitivity of each parameter as well as the associated effects on the 3D stability number. In this study, all numerical results are used as training data in the multivariate adaptive regression splines (MARS) model, and a simple empirical equation is established for the 3D undrained slope considering anisotropy and heterogeneity. To the authors' best knowledge, this is the first time to present rigorous LB and UB stability solutions of 3D undrained slopes in anisotropic and heterogenous clay. This is also the first time to apply MARS model (a curve-based machine learning method) to analyzing the output numerical results. This study would be of great interest to practitioners.

2. Problem statement and numerical modeling

Fig. 1 shows the geometry of a 3D slope that is defined by slope angle (β), slope height (H), model depth (d), and model length (L). A potential failure mechanism (the hatch area) of the 3D slope is also shown in this figure. The soil mass of the 3D slope is assumed to be perfectly plastic, and the failure criterion of soil is based on the AUS failure criterion proposed by Krabbenhoft et al. (2019).

Anisotropy refers to the material property that is dependent on the loading direction. In AUS model, three input strength parameters are used to describe the behavior of clay, including the undrained shear strength obtained from triaxial compression test (s_{uc}), triaxial extension test (s_{ue}), and direct simple shear test (s_{us}). Three strength parameters are further normalized into the following dimensionless anisotropic parameters: $r_e = s_{ue}/s_{uc}$ and $r_s = s_{us}/s_{uc}$. Fig. 2 presents the problem statement of anisotropic and heterogenous clays. Note that in this paper using AUS, soil strengths obtained from different loading tests are considered. Nevertheless, they are not used along the potential slip surface, which cannot reflect real soil anisotropy. Ideally, anisotropy should refer to different behaviors for different directions of the material. The soil may not respond in the same way to a compression loading as it does to an extension loading.

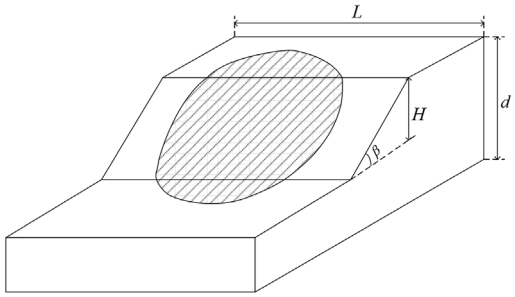

Fig. 1. 3D slope geometry.

According to Krabbenhoft et al. (2019), the value of r_s can be determined from r_e using the harmonic mean as

$$r_s = \frac{2r_e}{1+r_e} \tag{1}$$

Therefore, the anisotropic behavior of clay can be studied using the parameter r_e. Note that the value of r_e varies from 0.5 to 1, whilst $r_e = 1$ indicates an isotropic state of Tresca failure criterion (Fig. 3).

Coupled with the anisotropy, the heterogeneous behavior of clay is investigated using three anisotropic undrained shear strength parameters that increase with depth by

$$s_{ue}(z) = s_{ue0} + r_e \rho z \tag{2}$$

$$s_{us}(z) = s_{us0} + r_s \rho z \tag{3}$$

$$s_{uc}(z) = s_{uc0} + \rho z \tag{4}$$

where s_{ue0}, s_{us0} and s_{uc0} are the anisotropic undrained shear strengths at the ground level; z denotes the depth from the ground surface; and ρ is the linear gradient (in kPa/m) (Fig. 2).

The stability solutions of 3D slopes in anisotropic and heterogenous clays are expressed using the dimensionless approach as stated in Butterfield (2009), which is a function of five dimensionless parameters as

$$N_\rho = \frac{\gamma HF}{s_{uc0}} = f\left(\beta, \frac{L}{H}, \frac{d}{H}, r_e, \lambda_{cp} = \frac{\rho HF}{s_{uc0}}\right) \tag{5}$$

where N_ρ is the 3D slope stability number, β is the slope angle, L/H is the length factor, d/H is the depth factor, $\lambda_{cp} = \rho HF/s_{uc0}$ is the normalized shear strength gradient, and F is the factor of safety. The proposed parametric study is for: (1) $\beta = 15°, 30°, 45°, 60°$; (2) $L/H = 1, 2, 3, 5$; (3) $d/H = 1, 2, 3, 5$; (4) $r_e = 0.5, 0.6, 0.7, 0.8, 0.9, 1$; and (5) $\lambda_{cp} = 0, 0.2, 0.4, 0.6, 0.8, 1, 2$.

The FELA software OptumG3 (OptumCE, 2020) is used to produce stability solutions. To enhance the numerical confidence, both LB and UB solutions are presented. For improving the computational efficiency, the automatically adaptive mesh refinement technique in OptumG3 is adopted (Ciria et al., 2008). Five iterations of the adaptive meshing are used, where the number of elements is set to be increased from 5000 to 10,000 (Keawsawasvong and Lai, 2021; Keawsawasvong, 2021), with more elements being used near high plastic zones.

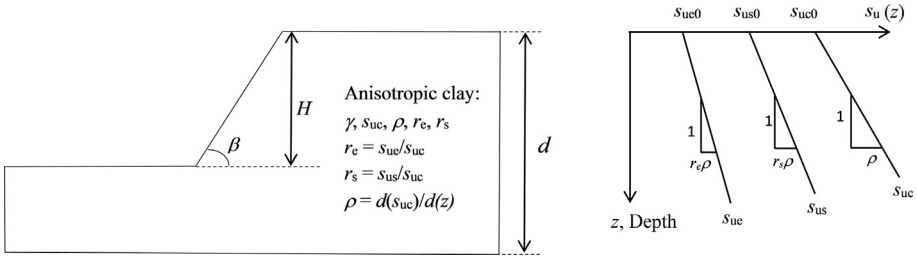

Fig. 2. Soil anisotropy (left) and increasing strength with depth (right).

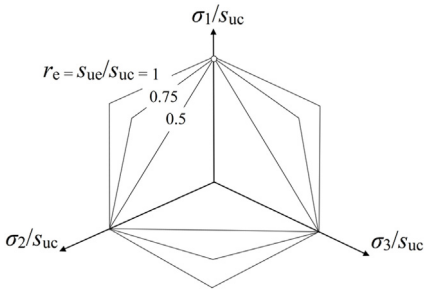

Fig. 3. GT yield surface in the AUS.

From the modeling aspect, it is vital to note that either an artificial "forced" boundary or a local 3D loading is needed to simulate a 3D slope study. This is because the proposed 3D geometry itself is a plane strain problem under gravity. To further explain this, Fig. 4 presents a comparison study of associated failure mechanisms under three scenarios. Note that the colored contours are representative of non-zero power dissipation, indicating the potential failure mechanism. The absolute values are neither real nor important in such a perfectly plastic soil model.

Fig. 4a depicts the case of a standard 2D slope under plane strain conditions (2D_PS), whilst Fig. 4b has a 3D slope geometry without the "forced" boundary (called 3D plane strain or 3D_PS). In Fig. 4a, all boundaries of the 2D_PS model are fixed in the *x*- and *y*-directions except for the face and the ground surface sides, which are free to move. For the 3D_PS in Fig. 4b, the boundary conditions are specified as follows: the bottom, front and back sides are fixed in the *x*-, *y*- and *z*-directions; the face and the ground sides are free. Note that both the left- and right-hand sides are fixed in the *x*-direction only, representing the symmetrical boundary conditions.

Fig. 4c is considered an "actual" 3D slope under soil gravity. The boundary conditions are the same as those in 3D_PS except for the left-hand side now being fixed in the *x*-, *y*- and *z*-directions. The right-hand side boundary remains as "fix *x*", giving a symmetrical condition for the slope, and therefore a 3D response is yielded.

Fig. 5 shows the relationship between stability number N_ρ and shear strength gradient ratio λ_{cp} for a 3D slope analysis considering the effect of L/H (Figs. 1 and 4c). Numerical results have shown that an increase of L/H results in a decrease in the stability number. Indeed, when L/H is large, such as $L/H = 15$, the stability numbers should be close to those of either 3D_PS or 2D_PS. As expected, the stability numbers of 3D_PS and 2D_PS are nearly identical. The study has greatly enhanced the confidence in modeling and has concluded the use of the model in Fig. 4c for all later analyses of the 3D slopes in anisotropic and heterogenous clays.

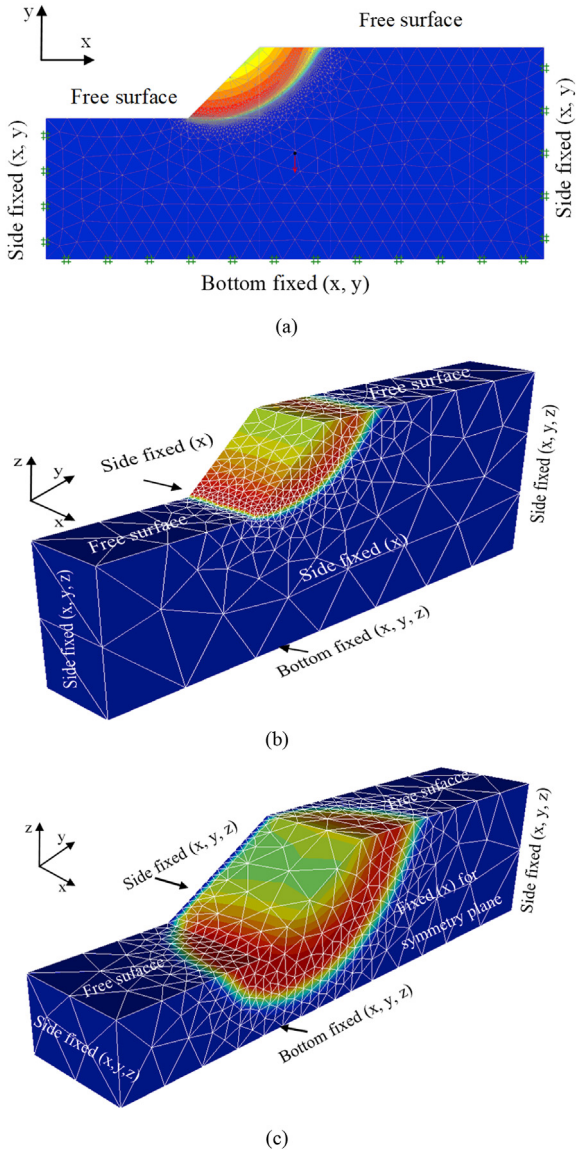

Fig. 4. Comparison of failure mechanisms in different models: (a) 2D_PS, (b) 3D_PS, (c) 3D.

3. MARS model

Owing to the complexity in considering the effects of five dimensionless parameters on the stability of the 3D anisotropic and heterogeneous slope, it is important to investigate the sensitivity of each parameter to the stability. An empirical equation considering all dimensionless design parameters is essential in assisting slope designs. Hence, the MARS model is adopted in this research.

The MARS analysis is a nonlinear regression method that can be used in data analysis of various geotechnical problems. Recently, Lai

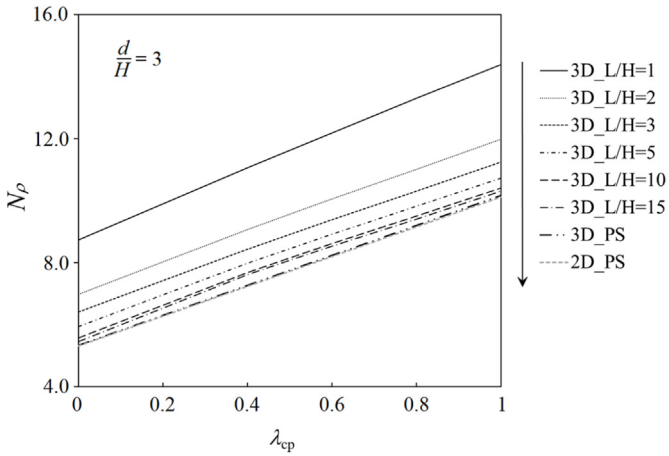

Fig. 5. Relationship between N_ρ and λ_{cp} for 2D and 3D slope analyses.

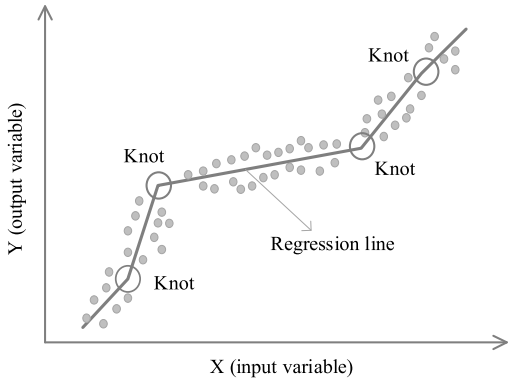

Fig. 6. The concept of MARS model.

et al. (2021) applied the MARS model to correlating the nonlinear relationship between a set of five dimensionless input variables and their respective output variables. The work was for studying the sensitivity of design parameters of two adjacent caissons. Zhang et al. (2019a) also used the MARS model to propose an empirical equation to predict the lateral displacement envelope for braced excavation in clays. Five input design parameters were considered in their study. MARS model has also been successfully applied to the induced uplift displacement of tunnels under earthquake loading (Zheng et al., 2019), as well as the embankment stability problem (Zhou et al., 2021). MARS model has also been applied to solving many other geotechnical problems (Zhang and Goh, 2013; Zhang, 2019; Hasanpour et al., 2020; Wang et al., 2020a; Qureshi et al., 2021; Lai et al., 2022c; Yodsomjai et al., 2022).

In comparison to other machine learning approaches, i.e. artificial neural network (Armaghani et al., 2019; Zhang et al., 2019b; Miah, 2021; Keawsawasvong et al., 2022b; Khajehzadeh et al., 2022a, b), extreme learning machine (Jamei et al., 2021; Bardhan et al., 2022), support vector regression (Alkroosh et al., 2015; Zhang et al., 2020, 2022), stochastic gradient boosting trees (Raja and Shukla, 2021), and XGBoost (Wang et al., 2020b; Zhang et al., 2021), MARS model is well known for its effectiveness (Wu and Fan, 2019; Raja and Shukla, 2021). MARS is also highly adaptive since it does not need any assumptions about the underlying functional relationships between input and output parameters (Zhang et al., 2020). Using a series of piecewise linear functions (splines) with different gradients to demonstrate nonlinear relationships between input parameters and output results, MARS is well suited for high-dimensional problems (i.e. five inputs in this study). It can be viewed as a generalization of stepwise linear regression, as shown in Fig. 6. The chosen split point (or the knot) is used to connect different splines. Better flexibility is provided in capturing the nonlinear regression process using the "knots". The fitted basic functions (BFs) presented for the splines are optimized in the adaptive regression algorithm that is presented as follows:

$$BF = \max(0, x-t) = \begin{cases} x-t \ (\text{if } x > t) \\ 0 \quad (\text{otherwise}) \end{cases} \tag{6}$$

where x is an input variable and t is a threshold value.

To illustrate the relationship between input and output parameters, an empirical equation is determined by combining all linear BFs as

$$f(x) = a_0 + \sum_{n=1}^{N} a_n g_n(x) \tag{7}$$

where a_0 is the constant, N is the number of BFs, g_n is the nth BF, and a_n is the coefficient of g_n.

In summary, MARS model is built by a two-step procedure. The first (or called "forward") step is to provide BFs as well as to find their potential knots to optimize the model performance and fitting accuracy. It often creates an over-fitted model using all input parameters. The second (or "backward") step uses a pruning algorithm based on the generalized cross validation (GCV) value to remove the least effective terms to obtain the optimal model. The GCV value can be determined by

$$GCV = \frac{RMSE}{[1-(N-hN)/R]^2} \tag{8}$$

where $RMSE$ is the root mean square error for the training dataset, h is the penalty factor, and R is the number of data points.

The increase in GCV values between the pruned model and the over-fitted model is considered as an important measure of the removed variable (Steinberg et al., 1999; Gan et al., 2014). The score of the ith parameter is represented by the relative importance index (RII) and determined by

$$RII(i) = \frac{\Delta g(i)}{\max\{\Delta g(i), \Delta g(2), \Delta g(3), \ldots, \Delta g(n)\}} \tag{9}$$

where Δg is the increase in GCV when the ith parameter is deleted. The higher the GCV rises, the more significant the deleted parameter is.

4. Validation, results and discussion

To verify the present FELA solutions, Fig. 7 presents the stability number N_ρ between the present study and Li et al. (2010) for the isotropic slope ($r_e = 1, \beta = 15°, d/H = 1, L/H = 1, 2, 3, 5$). Note that the FELA solution is presented using the average of LB and UB solutions. Numerical results have shown that N_ρ increases linearly with the increase in λ_{cp}, and our averaged LB and UB results are close to their LB ones. This observation applies to all values of L/H. It can therefore be concluded that the numerical confidence has been greatly improved using the latest AUS model in OptumG3. Following this validation, the 3D effects of the five dimensionless input parameters (β, d/H, L/H, λ_{cp}, r_e) on the stability numbers of anisotropic and heterogeneous slopes are investigated (Figs. 8–17).

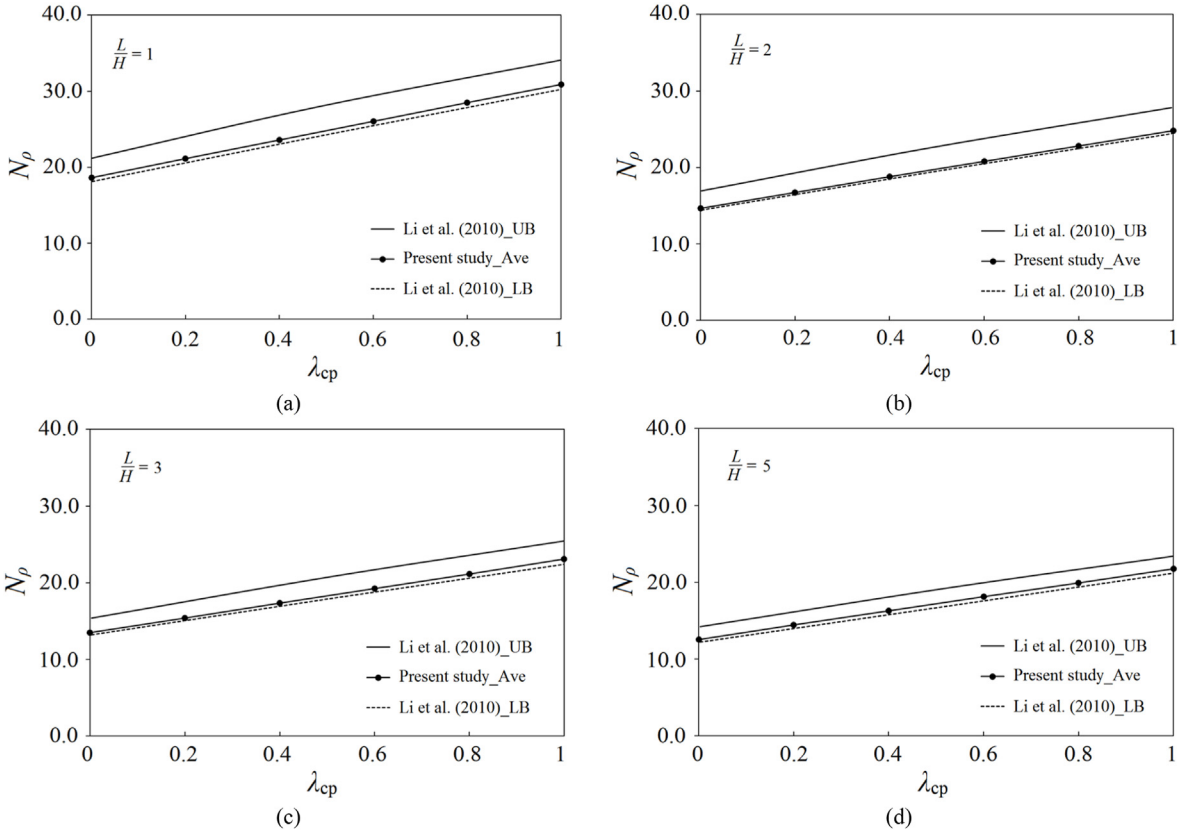

Fig. 7. Relationship between stability number N_ρ and strength gradient ratio λ_{cp} under different values of L/H.

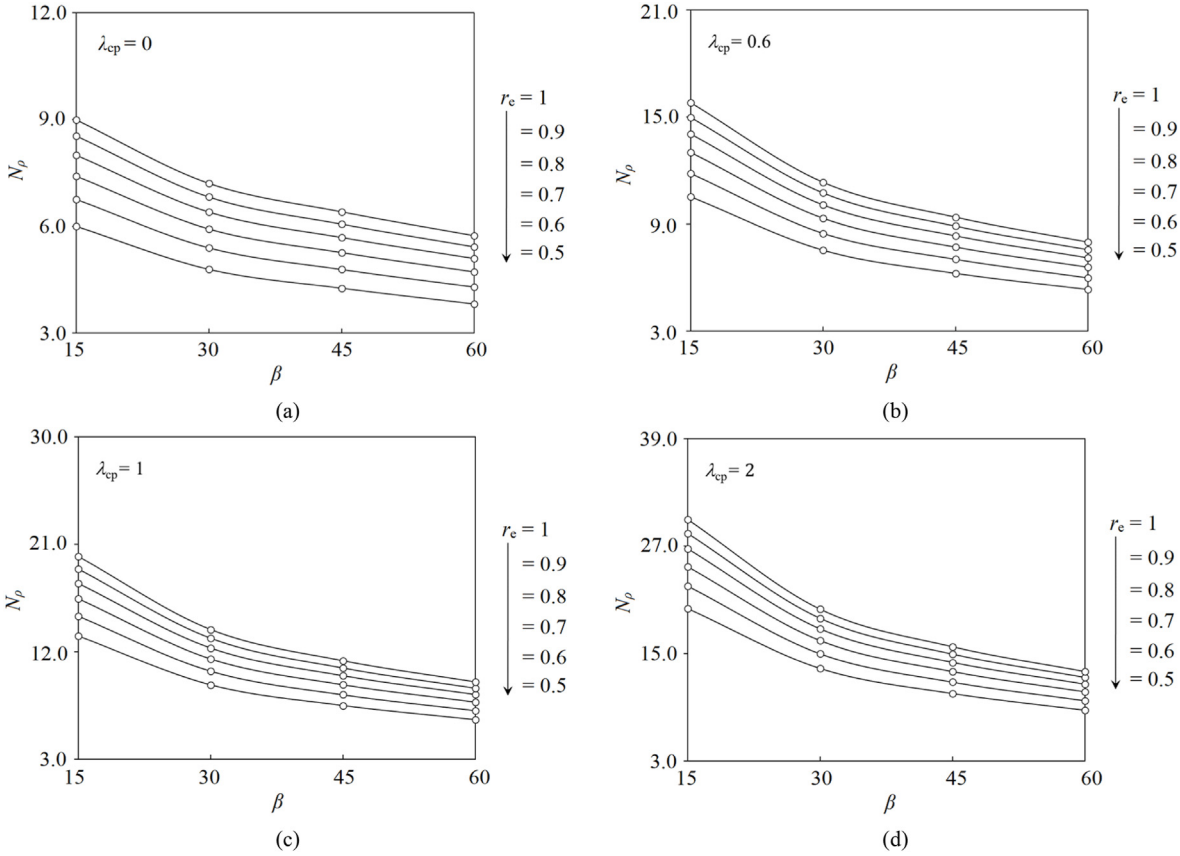

Fig. 8. Relationship between stability number N_ρ and various slope angles (β = 15°, 30°, 45°, 60°) and soil anisotropy ratios (r_e = 0.5, 0.6, 0.7, 0.8, 0.9, 1) at increasing strength gradient ratio (λ_{cp} = 0, 0.6, 1, 2).

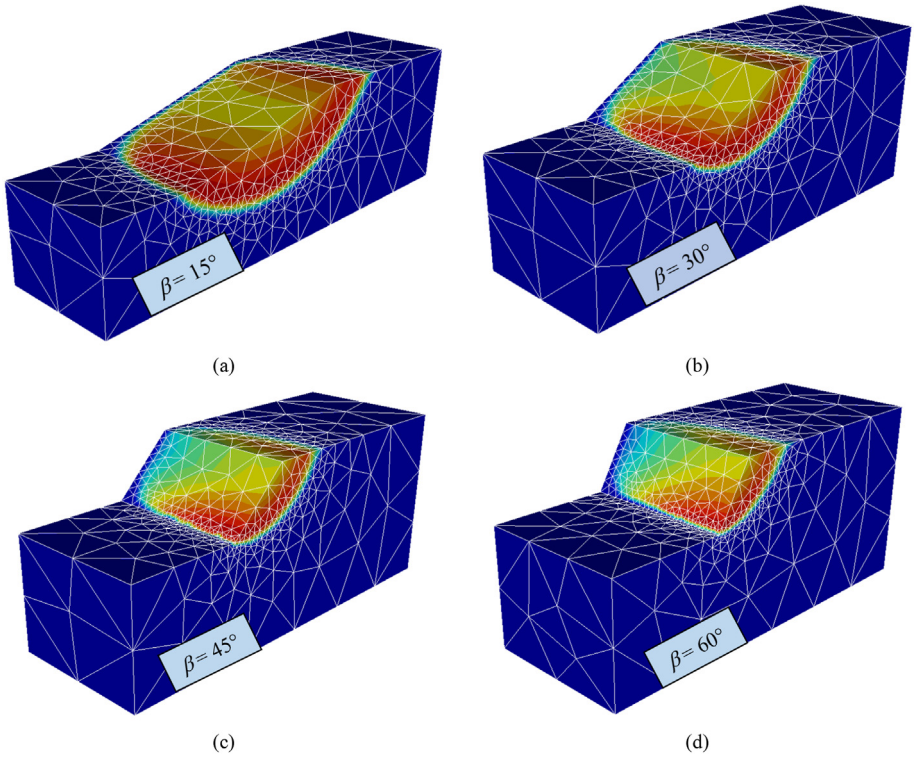

Fig. 9. Comparison of failure mechanisms under different values of β.

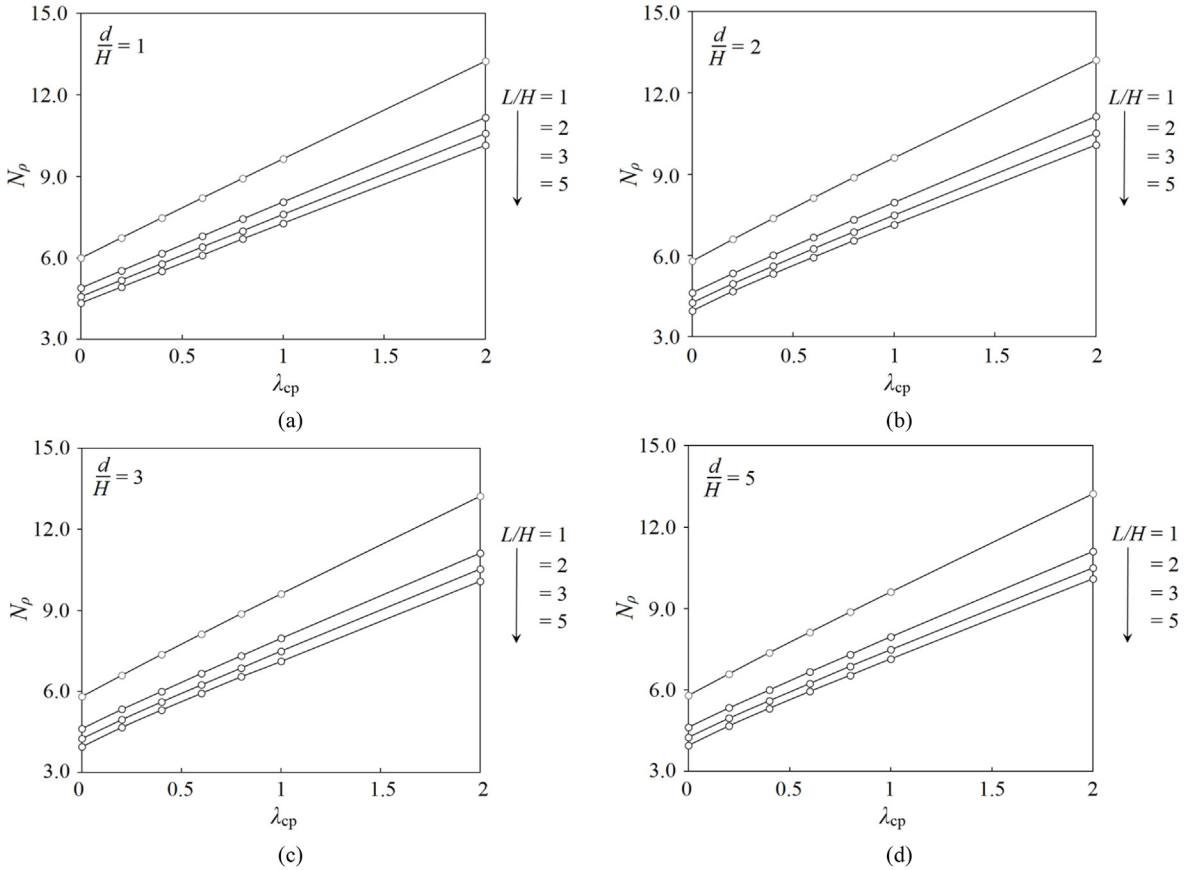

Fig. 10. Effect of soil strength gradient ratio λ_{cp} on the stability number N_ρ for various values of L/H and d/H.

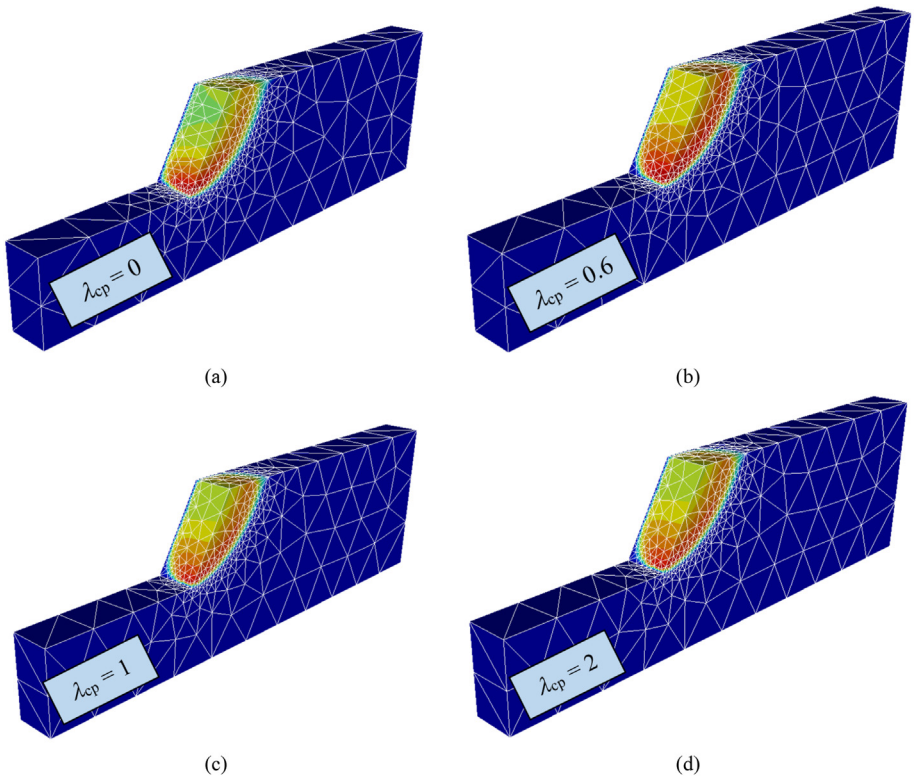

Fig. 11. Comparison of failure mechanisms under different values of λ_{cp}.

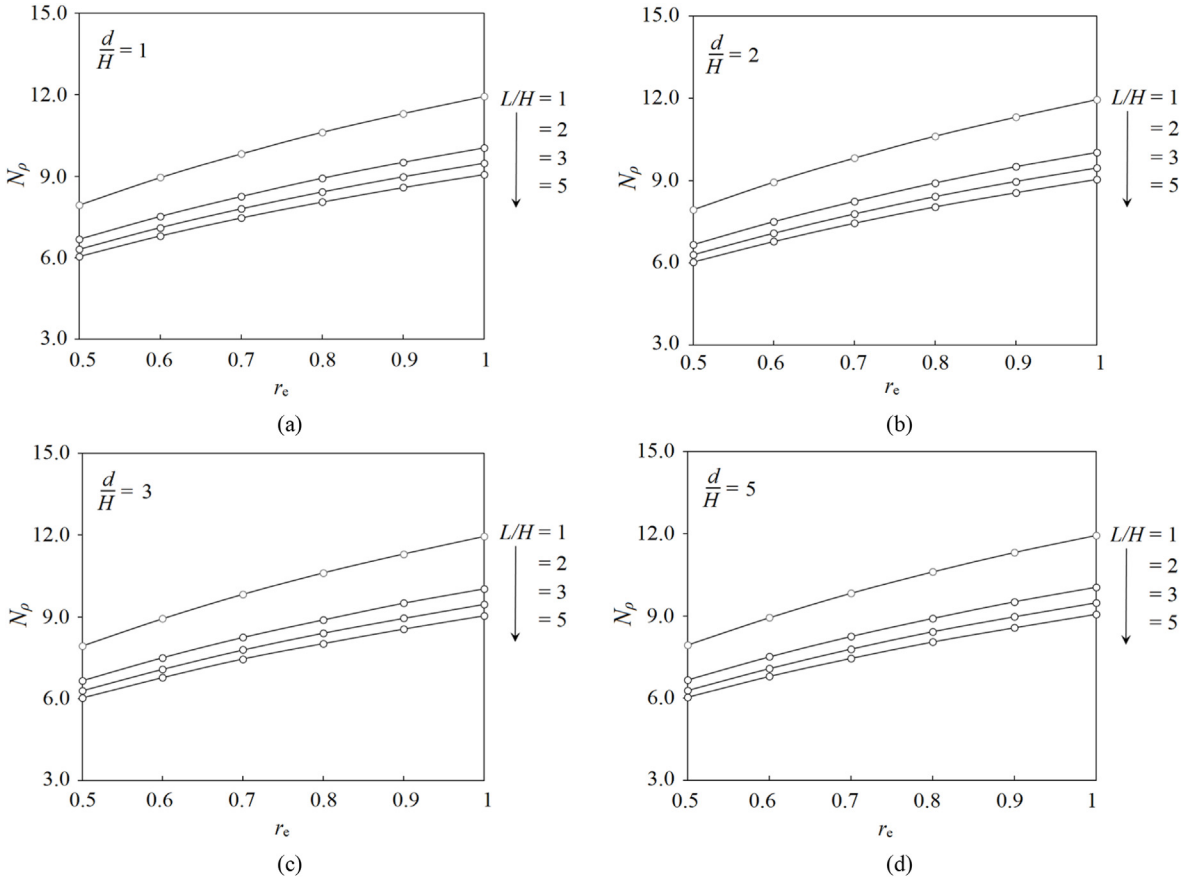

Fig. 12. Relationship between N_ρ and r_e ($\beta = 60°$, $\lambda_{cp} = 1$, $d/H = 1, 2, 3, 5$).

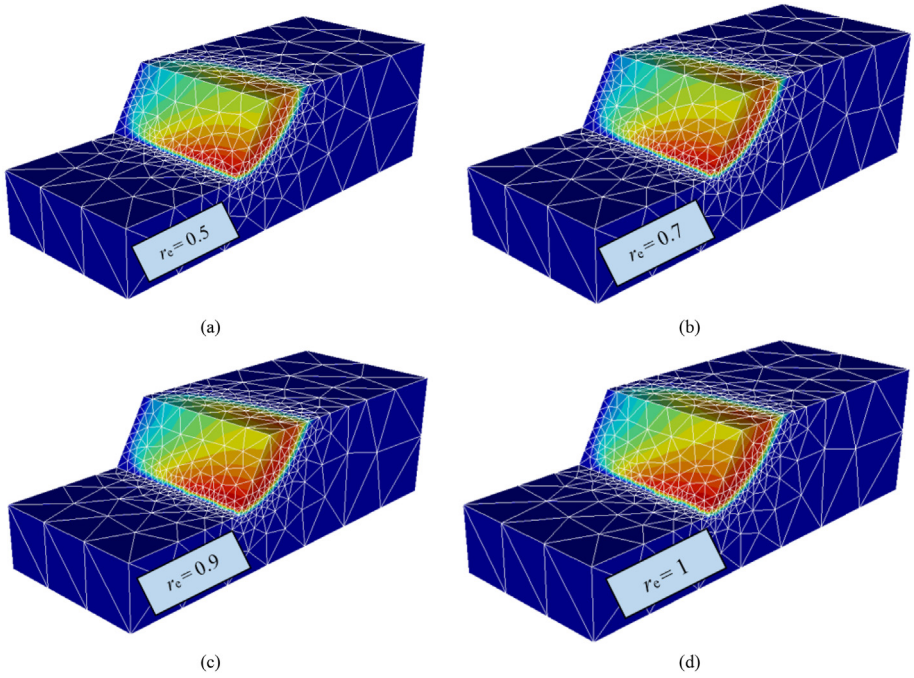

Fig. 13. Comparison of failure mechanisms under different values of r_e.

Fig. 8 shows the relationship between stability number N_ρ and various slope angles (β = 15°, 30°, 45°, 60°) and soil anisotropy ratios (r_e = 0.5, 0.6, 0,7, 0.8, 0.9, 1) at increasing strength gradient ratio (λ_{cp} = 0, 0.6, 1, 2). The chosen geometric parameters for the study are $L/H = 3$ and $d/H = 3$. Results show that an increase of the slope angle β yields to a nonlinear decrease of the stability number N_ρ for all investigated values of λ_{cp}. It is not surprised to see that an increase of slope angle results in a less stable slope. Four selected failure mechanisms (β = 15°, 30°, 45°, 60°) are presented in Fig. 9. They are for $r_e = 0.8$, $\lambda_{cp} = 1$, $L/H = 5$ and $d/H = 3$. As the slope angle

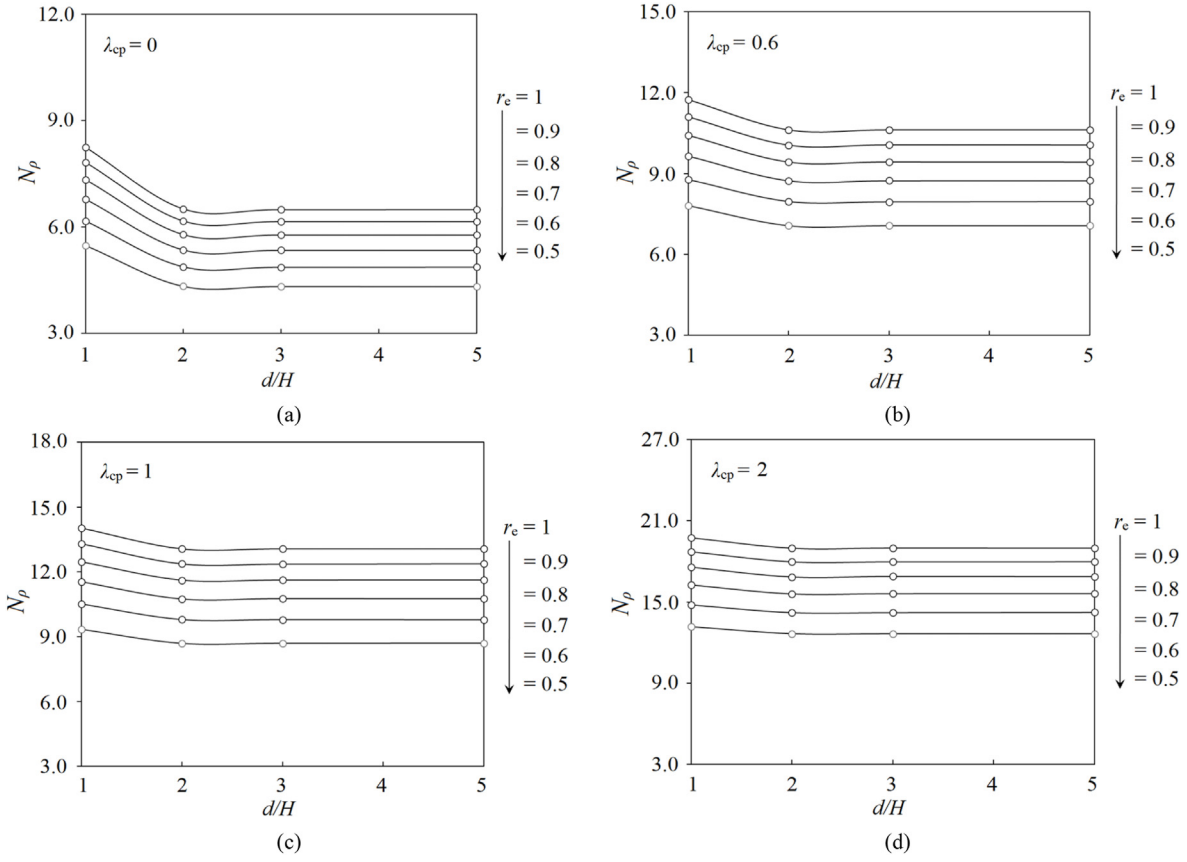

Fig. 14. Relationship between N_ρ and d/H (β = 30°, $L/H = 5$, λ_{cp} = 0, 0.6, 1, 2).

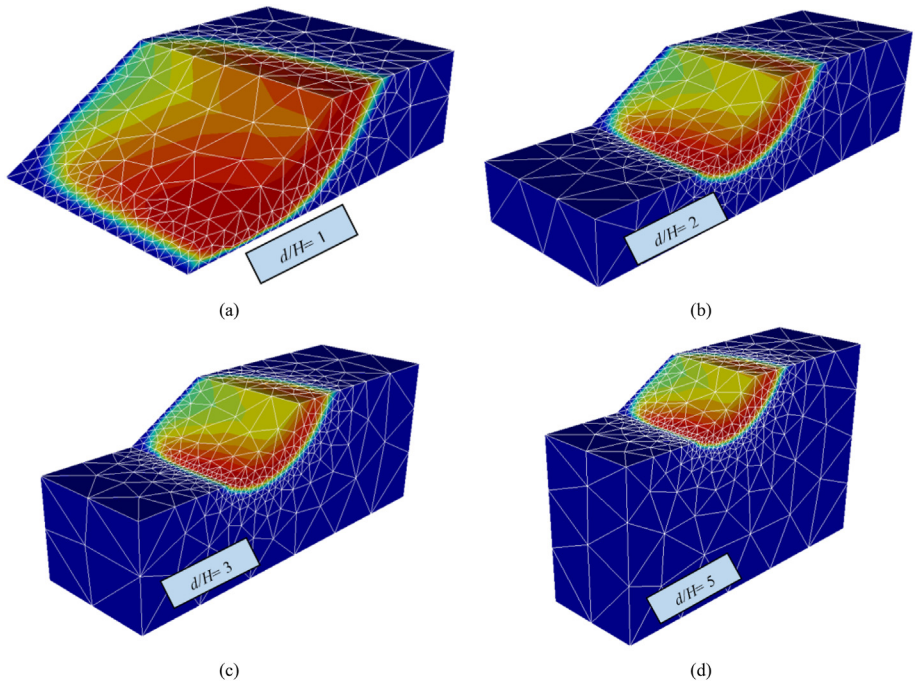

Fig. 15. Comparison of failure mechanisms under different values of d/H.

increases from 15° to 60°, the overall volume of the failure zone becomes smaller, and the type of failure changes from a base-failure mode to a toe-failure or a face-failure mode.

The effect of soil strength gradient ratio λ_{cp} on the stability number N_ρ for various L/H values is shown in Fig. 10. The selected presentation is for $\beta = 45°$, $r_e = 0.5$, and $d/H = 1, 2, 3, 5$. A linear increasing relationship between stability number N_ρ and soil strength gradient ratio λ_{cp} is obtained for all cases ($d/H = 1, 2, 3, 5$, $L/H = 1, 2, 3, 5$). Fig. 11 shows a comparison of the failure mechanism of the four different strength gradient ratios ($\lambda_{cp} = 0, 0.6, 1, 2$). These

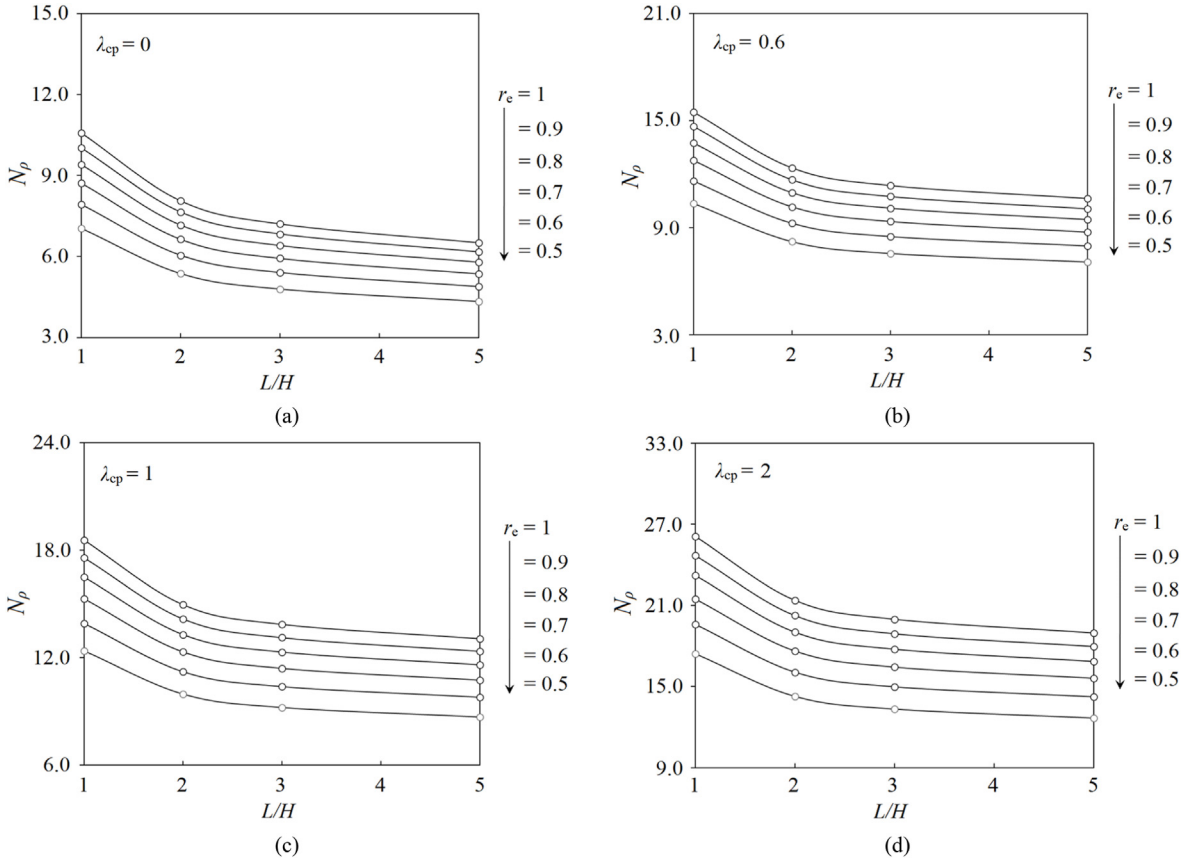

Fig. 16. Relationship between N_ρ and L/H ($\beta = 30°$, $d/H = 2$, $\lambda_{cp} = 0, 0.6, 1, 2$).

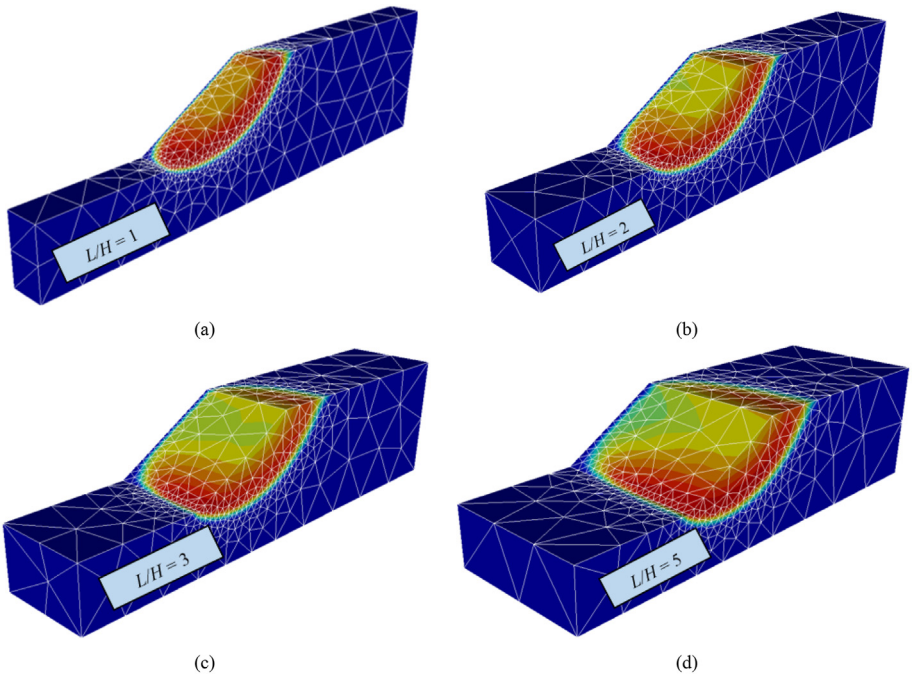

Fig. 17. Comparison of failure mechanisms under different values of L/H.

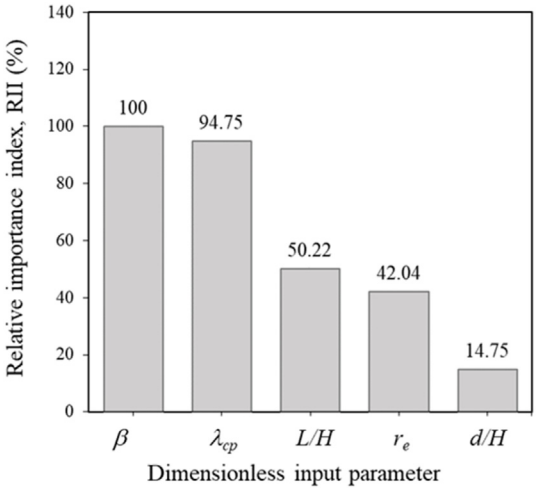

Fig. 18. Sensitive analysis of five parameters.

Table 1
BFs and the empirical equations for N_ρ.

BF	Equation	BF	Equation
BF1	max [0, $(\beta - 30)$]	BF15	max [0, $(0.8 - r_e)$] × BF3
BF2	max [0, $(30 - \beta)$]	BF16	max [0, $(\beta - 30)$] × BF15
BF3	max [0, $(\lambda_{cp} - 0)$]	BF17	max [0, $(30 - \beta)$] × BF15
BF4	max [0, $(L/H - 2)$]	BF18	max [0, $(3 - L/H)$] × BF3
BF5	max [0, $(2 - L/H)$]	BF19	max [0, $(\beta - 45)$] × BF18
BF6	max [0, $(r_e - 0.7)$]	BF20	max [0, $(45 - \beta)$] × BF18
BF7	max [0, $(0.7 - r_e)$]	BF21	max [0, $(r_e - 0.5)$] × BF11
BF8	max [0, $(\lambda_{cp} - 0.6)$] × BF2	BF22	max [0, $(2 - d/H)$] × BF11
BF9	max [0, $(0.6 - \lambda_{cp})$] × BF2	BF23	max [0, $(L/H - 2)$] × BF1
BF10	max [0, $(L/H - 2)$] × BF2	BF24	max [0, $(2 - L/H)$] × BF1
BF11	max [0, $(2 - L/H)$] × BF2	BF25	max [0, $(\lambda_{cp} - 0.6)$] × BF12
BF12	max [0, $(2 - d/H)$] × BF2	BF26	max [0, $(0.6 - \lambda_{cp})$] × BF12
BF13	max [0, $(\lambda_{cp} - 0)$] × BF1	BF27	max [0, $(\beta - 15)$] × BF6
BF14	max [0, $(r_e - 0.8)$] × BF3		

Note: The empirical equation for N_ρ: $N_\rho = 6.79127 - 0.0536684BF1 + 0.292989BF2 + 5.32605BF3 - 0.316594BF4 + 2.18929BF5 + 6.5277BF6 - 6.61517BF7 + 0.244203BF8 - 0.324137BF9 - 0.024708BF10 + 0.0839839BF11 + 0.188355BF12 - 0.0793451BF13 + 3.38076BF14 - 4.80313BF15 + 0.0958865BF16 - 0.298921BF17 + 0.196017BF18 + 0.0119605BF19 + 0.0388073BF20 + 0.372231BF21 - 0.0970221BF22 + 0.00465014BF23 - 0.0309415BF24 - 0.0455977BF25 + 0.108208BF26 - 0.083836BF27$.

plots are based on the selected case of $\beta = 45°$, $r_e = 0.5$, $d/H = 2$ and $L/H = 1$. Interestingly, it was found that the overall failure zone does not differ much in size and pattern for all values of λ_{cp}. This can be understood through the theoretical background of the strength reduction method, in which the soil strength is reduced uniformly during the computational process for a final outcome of the factor of safety. Therefore, the failure mechanism does not change with varied values of λ_{cp}.

Similarly, a slight convex relationship between stability number N_ρ and anisotropic ratio r_e is shown in Fig. 12. In general, N_ρ increases with increasing value of r_e for all values of L/H and d/H. Similarly, minor differences in failure mechanism are observed with the different r_e ratios in Fig. 13. Similar observation was also reported by Keawsawasvong and Ukritchon (2022). It is therefore concluded that the effect of r_e on the overall failure mechanism is insignificant.

The relationships between stability number N_ρ and depth ratio of d/H for various soil strength gradient ratios ($\lambda_{cp} = 0$, 0.6, 1, 2) and anisotropic ratios ($r_e = 0.5$, 0.6, 0.7, 0.8, 0.9, 1) are shown in Fig. 14. The study is for the case of $\beta = 30°$ and $L/H = 5$. It is to be noted that the stability number N_ρ decreases with increasing values of depth ratio (d/H). Depending on the value of d/H and λ_{cp}, N_ρ becomes constant, and it is no longer dependent on the depth ratio (d/H). This can be self-explained by inspecting the failure mechanism plots in Fig. 15. There is no change of the failure zone for cases with $d/H > 2$.

Fig. 16 presents the effect of L/H on the stability number N_ρ. Four various strength gradient ratios ($\lambda_{cp} = 0$, 0.6, 1, 2) and five anisotropic ratios ($r_e = 0.5$, 0.6, 0.7, 0.8, 0.9, 1) are reported and the chosen case is for $\beta = 30°$ and $d/H = 2$. Numerical results have shown a nonlinear relationship between N_ρ and L/H. An increase of L/H results in a nonlinear decrease of N_ρ. Depending on the value of

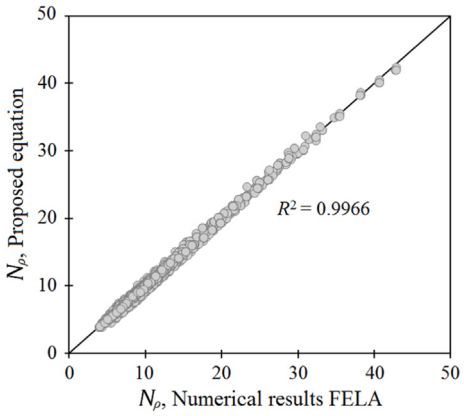

Fig. 19. Comparison of N_ρ between the proposed equation and FELA results.

λ_{cp} and r_e, N_ρ tends to approach a constant value, indicating that the solution is close to a plane strain one. The larger the L/H, the smaller the stability number N_ρ, and the closer the results of N_ρ to a plane strain one. This has also been discussed in Figs. 4 and 5. The failure mechanisms of four different values of L/H are shown in Fig. 17, where less boundary effect is depicted in the case of $L/H = 5$.

5. Sensitive analysis and empirical equation by MARS model

In this study, all 2688 stability numbers (Tables A1-A4 in Appendix), corresponding to the input values of dimensionless parameters (i.e. β, d/H, L/H, λ_{cp}, r_e), are used as the training data for the sensitivity analysis in MARS model. The outcome of the sensitivity study is presented in Fig. 18, where the relative importance index (RII) is shown for each dimensionless input parameter. The respective RII values for β, λ_{cp}, L/H, r_e and d/H are 100%, 94.75%, 50.22%, 42.04% and 14.75%, respectively. RII of 100% means that the slope angle β is the most sensitive parameter that could affect the design outcome. λ_{cp}, with a RII of 94.75%, would also indicate that the strength gradient ratio has a significant role in slope stability performance. L/H and r_e are considered as moderate, though cannot be ignored in practice, whilst d/H is of less significance.

Table 1 shows a comprehensive output of the 27 BFs considering the effects of all five investigated parameters. The nonlinear relationship between the five input parameters and output stability numbers is also presented in Table 1. To verify the accuracy of the proposed empirical equation, a comparison between the stability numbers calculated from the proposed equation and those from the actual FELA results is shown in Fig. 19. Good agreement is displayed with the coefficient of determination $R^2 = 0.9966$. It can therefore be concluded that the proposed equation based on the MARS model can be an effective and efficient tool in practice.

6. Conclusions

This paper has investigated the undrained stability of 3D slopes in anisotropic and heterogenous clay using advanced LB and UB FELA. A set of five dimensionless parameters including slope angle β, depth ratio (d/H), length ratio (L/H), shear strength gradient ratio (λ_{cp}), and anisotropic strength ratio (r_e) is considered in the analysis to examine their influences on the stability numbers N_ρ and the associated failure mechanisms. The sensitivity of each parameter is also analyzed using an MARS model, where both the RII and the empirical equation are determined. The following conclusions can be drawn:

(1) The increases in β, L/H and d/H result in a nonlinear decrease of the stability number N_ρ, whilst the increases in λ_{cp} and r_e produce an increase in N_ρ.
(2) The resulting failure mechanisms are largely affected by the changes in β and L/H, rather than by the other three parameters: λ_{cp}, r_e and d/H.
(3) Based on the MARS analysis, the slope angle β is the most important parameter that affects the stability performance. This is followed by λ_{cp}, L/H, r_e and d/H with respective RII of 94.75%, 50.22%, 42.04% and 14.75%.
(4) A highly accurate empirical equation is developed based on the MARS analysis, and it is well recognized as an effective and efficient tool in practice.

The numerical model is found to be well suited to solving the proposed problem owing to its numerical efficiency. It is recommended that the current work can be extended to 3D random field analysis in the future considering the spatially variable soils as well as for cohesive-frictional soils.

The LB and UB FELA are used to analyze the factor of safety for 3D slope in anisotropic and heterogenous clay. Although this is the first time that the influences of the 3D geometries of slope and anisotropic behaviors of clay are carefully investigated, it is limited by certain assumptions and should be investigated further as follows:

(1) All of the proposed design charts are restricted with the assumption of undrained soil conditions, which cannot be used in drained soil conditions.
(2) All of proposed design charts and equation built by MARS model for the factor of safety for 3D slope in anisotropic and heterogenous clay correspond to the ranges of investigated input parameters. The output prediction may be inaccurate if the input values are out of these ranges.

Declaration of competing interest

The authors declare that they have no known competing financial interests or personal relationships that could have appeared to influence the work reported in this paper.

Acknowledgments

We would like to thank Ho Chi Minh City University of Technology (HCMUT), VNU-HCM for the support of time and facilities for this study.

Appendix A. Supplementary data

Supplementary data to this article can be found online at https://doi.org/10.1016/j.jrmge.2022.05.016.

References

Alkroosh, I.S., Bahadori, M., Nikraz, H., Bahadori, A., 2015. Regressive approach for predicting bearing capacity of bored piles from cone penetration test data. J. Rock Mech. Geotech. Eng. 7 (5), 584–592.
Ardestani, A., Amini, M., Esmaeili, K., 2021. A two-dimensional limit equilibrium computer code for analysis of complex toppling slope failures. J. Rock Mech. Geotech. Eng. 13 (1), 114–130.
Armaghani, D.J., Koopialipoor, M., Marto, A., Yagiz, S., 2019. Application of several optimization techniques for estimating TBM advance rate in granitic rocks. J. Rock Mech. Geotech. Eng. 11 (4), 779–789.
Azarafza, M., Akgün, H., Ghazifard, A., Asghari-Kaljahi, E., Rahnamarad, J., Derakhshani, R., 2021. Discontinuous rock slope stability analysis by limit equilibrium approaches–a review. Int. J. Digit. Earth 14 (12), 1918–1941.

Azzouz, A.S., Baligh, M.M., 1978. Three-dimensional Stability of Slopes. Research Rep, R7vols. 8–8. Department of Civil Engineering, Massachusetts Institute of Technology, Cambridge, MA, UK. Order No. 595.

Baligh, M.M., Azzouz, A.S., 1975. End effects on stability of cohesive slopes. J. Geotech. Eng. Div. 101 (11), 1105–1117.

Bardhan, A., Kardani, N., Alzoùbi, A.K., Roy, B., Samui, P., Gandomi, A.H., 2022. Novel integration of extreme learning machine and improved Harris hawks optimization with particle swarm optimization-based mutation for predicting soil consolidation parameter. J. Rock Mech. Geotech. Eng. https://doi.org/10.1016/j.jrmge.2021.12.018.

Bishop, A.W., 1955. The use of the slip circle in the stability analysis of slopes. Geotechnique 5 (1), 7–17.

Butterfield, R., 2009. Dimensional analysis for geotechnical engineering. Geotechnique 49 (2), 357–366.

Casagrande, A., Carillo, N., 1944. Shear Failure of Anisotropic Soils. Harvard Graduate School of Engineering, Harvard University, Cambridge, MA, USA.

Chai, J., Igaya, Y., Hino, T., Carter, J., 2013. Finite element simulation of an embankment on soft clay—case study. Comput. Geotech. 48 (1), 117–126.

Chang, M., 2002. A 3D slope stability analysis method assuming parallel lines of intersection and differential straining of block contacts. Can. Geotech. J. 39 (4), 799–811.

Ciria, H., Peraire, J., Bonet, J., 2008. Mesh adaptive computation of upper and lower bounds in limit analysis. Int. J. Numer. Methods Eng. 75 (8), 899–944.

Gan, Y., Duan, Q., Gong, W., et al., 2014. A comprehensive evaluation of various sensitivity analysis methods: a case study with a hydrological model. Environ. Model. Software 51, 269–285.

Gens, A., Hutchinson, J.N., Cavounidis, S., 1988. Three-dimensional analysis of slides in cohesive soils. Geotechnique 38 (1), 1–23.

Ghadrdan, M., Dyson, A.P., Shaghaghi, T., Tolooiyan, A., 2021. Slope stability analysis using deterministic and probabilistic approaches for poorly defined stratigraphies. Geomech. Geophys. Geo. 7 (1), 1–17.

Guo, M., Ge, X., Wang, S., 2011. Slope stability analysis under seismic load by vector sum analysis method. J. Rock Mech. Geotech. Eng. 3 (3), 282–288.

Griffiths, D., Lane, P., 1999. Slope stability analysis by finite elements. Geotechnique 49 (3), 387–403.

Griffiths, D., Marquez, R., 2007. Three-dimensional slope stabilityanalysis by elasto-plastic finite elements. Geotechnique 57 (6), 537–546.

Hasanpour, R., Rostami, J., Schmitt, J., Ozcelik, Y., Sohrabian, B., 2020. Prediction of TBM jamming risk in squeezing grounds using Bayesian and artificial neural networks. J. Rock Mech. Geotech. Eng. 12 (1), 21–31.

Janbu, N., 1973. Slope Stability Computations. John Wiley and Sons, New York, USA.

Jamei, M., Hasanipanah, M., Karbasi, M., et al., 2021. Prediction of flyrock induced by mine blasting using a novel kernel-based extreme learning machine. J. Rock Mech. Geotech. Eng. 13 (6), 1438–1451.

Jearsiripongkul, T., Lai, V.Q., Keawsawasvong, S., Nguyen, T.S., Van, C.N., Thongchom, C., Nuaklong, P., 2022. Prediction of uplift capacity of cylindrical caissons in anisotropic and inhomogeneous clays using multivariate adaptive regression splines. Sustainability 14 (8), 4456.

Kainthola, A., Verma, D., Thareja, R., Singh, T.N., 2013. A review on numerical slope stability analysis. Int. J. Sci. Eng. Technol. Res. 2 (6), 1315–1320.

Kardani, N., Zhou, A., Nazem, M., Shen, S.L., 2021. Improved prediction of slope stability using a hybrid stacking ensemble method based on finite element analysis and field data. J. Rock Mech. Geotech. Eng. 13 (1), 188–201.

Keawsawasvong, S., 2021. Bearing capacity of conical footings on clays considering combined effects of anisotropy and non-homogeneity. Ships Offshore Struct. https://doi.org/10.1080/17445302.2021.1987110.

Keawsawasvong, S., Ukritchon, B., 2019a. Undrained basal stability of braced circular excavations in non-homogeneous clays with linear increase of strength with depth. Comput. Geotech. 115, 103180.

Keawsawasvong, S., Ukritchon, B., 2019b. Undrained stability of a spherical cavity in cohesive soils using finite element limit analysis. J. Rock Mech. Geotech. Eng. 11 (6), 1274–1285.

Keawsawasvong, S., Ukritchon, B., 2020. Design equation for stability of shallow unlined circular tunnels in Hoek-Brown rock masses. Bull. Eng. Geol. Environ. 79, 4167–4190.

Keawsawasvong, S., Lai, V.Q., 2021. End bearing capacity factor for annular foundations embedded in clay considering the effect of the adhesion factor. Int. J. Geosynth. Ground Eng. 7 (1), 1–10.

Keawsawasvong, S., Yoonirundorn, K., Senjuntichai, T., 2021. Pullout capacity factor for cylindrical suction caissons in anisotropic clays based on anisotropic undrained shear failure criterion. Transp. Infrastruct. Geotechnol. 8, 629–644, 2021.

Keawsawasvong, S., Ukritchon, B., 2021. Undrained stability of plane strain active trapdoors in anisotropic and non-homogeneous clays. Tunn. Undergr. Space Technol. 107, 103628.

Keawsawasvong, S., Shiau, J., 2022. Stability of active trapdoors in axisymmetry. Undergr. Space 7 (1), 50–57.

Keawsawasvong, S., Shiau, J., Ngamkhanong, C., Lai, V.Q., Thongchom, C., 2022a. Undrained stability of ring foundations: axisymmetry, anisotropy, and non-homogeneity. Int. J. GeoMech. https://doi.org/10.1061/(ASCE)GM.1943-5622.0002229.

Keawsawasvong, S., Seehavong, S., Ngamkhanong, C., 2022b. Application of artificial neural networks for predicting the stability of rectangular tunnel in Hoek-Brown rock masses. Front. Built Environ. 8, 837745.

Keawsawasvong, S., Ukritchon, B., 2022. Design equation for stability of a circular tunnel in an anisotropic and heterogeneous clay. Undergr. Space 7 (1), 76–93.

Khajehzadeh, M., Keawsawasvong, S., Nehdi, M.L., 2022a. Effective hybrid soft computing approach for optimum design of shallow foundations. Sustainability 14 (3), 1847.

Khajehzadeh, M., Taha, M.R., Keawsawasvong, S., Mirzaei, H., Jebeli, M., 2022b. An effective artificial intelligence approach for slope stability evaluation. IEEE Access 10, 5660–5671.

Krabbenhoft, K., Galindo-Torres, S.A., Zhang, X., Krabbenhøft, J., 2019. AUS: AUS strength model for clays. Int. J. Numer. Anal. Methods GeoMech. 43 (17), 2652–2666.

Krabbenhoft, K., Lyamin, A.V., 2015. Generalised Tresca criterion for undrained total stress analysis. Géotech. Lett. 5, 313–317.

Kumar, J., Samui, P., 2006. Stability determination for layered soil slopes using the upper bound limit analysis. Geotech. Geol. Eng. 24 (6), 1803–1819.

Ladd, C.C., 1991. Stability evaluations during stage construction. J. Geotech. Eng. 117 (4), 540–615.

Ladd, C.C., DeGroot, D.J., 2003. Recommended practice for soft ground site characterization". Arthur Casagrande Lecture. In: Proceedings of the 12th Panamerican Conference on Soil Mechanics and Geotechnical Engineering. Cambridge, MA, USA.

Lai, F., Zhang, N., Liu, S., Sun, Y., Li, Y., 2021. Ground movements induced by installation of twin large diameter deeply-buried caissons: 3D numerical modeling. Acta Geotechnica 16, 2933–2961.

Lai, V.Q., Nguyen, D.K., Banyong, R., Keawsawasvong, S., 2022a. Limit analysis solutions for stability factor of unsupported conical slopes in clays with heterogeneity and anisotropy. Int. J. Comput. Mater. Sci. Eng. 11 (1), 2150030–2150128.

Lai, V.Q., Banyong, B., Keawsawasvong, S., 2022b. Stability of limiting pressure behind soil gaps in contiguous pile walls in anisotropic clays. Eng. Fail. Anal. 134, 106049.

Lai, V.Q., Shiau, J., Keawsawasvong, S., Tran, D.T., 2022c. Bearing capacity of ring foundations on anisotropic and heterogenous clays ~ FEA, NGI-ADP, and MARS. Geotech. Geol. Eng. 40, 3913–3928.

Leshchinsky, D., Baker, R., 1986. Three-dimensional slope stability: end effects. Soils Found. 26 (4), 98–110.

Leshchinsky, D., Huang, C.C., 1992. Generalized slope stability analysis: interpretation, modification, and comparison. J. Geotech. Eng. 118 (10), 1559–1576.

Li, A.J., Merifield, R.S., Lyamin, A.V., 2009. Limit analysis solutions for three dimensional undrained slopes. Comput. Geotech. 36 (8), 1330–1351.

Li, A.J., Merifield, R.S., Lyamin, A.V., 2010. Three-dimensional stability charts for slopes based on limit analysis methods. Can. Geotech. J. 47 (12), 1316–1334.

Li, A.J., Merifield, R.S., Lin, H.D., Lyamin, A.V., 2014a. Trench stability under bentonite pressure in purely cohesive clay. Int. J. GeoMech. 151–157. https://doi.org/10.1061/(ASCE)GM.1943-5622.0000292.

Li, E., Zhuang, X., Zheng, W., Cai, Y., 2014b. Effect of graph generation on slope stability analysis based on graph theory. J. Rock Mech. Geotech. Eng. 6 (4), 380–386.

Lo, K.Y., 1965. Stability of slopes in anisotropic soils. J. Soil Mech. Found Div. 31, 85–106.

Loukidis, D., Bandini, P., Salgado, R., 2003. Stability of seismically loaded slopes using limit analysis. Geotechnique 53 (5), 463–480.

Lu, Y., 2015. Deformation and failure mechanism of slope in three dimensions. J. Rock Mech. Geotech. Eng. 7 (2), 109–119.

Ma, H., Luo, Q., Wang, T., Jiang, H., Lu, Q., 2021. Numerical stability analysis of piled embankments reinforced with ground beams. Transport. Geotechnics. 26, 100427.

Miah, M.I., 2021. Improved prediction of shear wave velocity for clastic sedimentary rocks using hybrid model with core data. J. Rock Mech. Geotech. Eng. 13 (6), 1466–1477.

Morgenstern, N., Price, V.E., 1965. The analysis of the stability of general slip surfaces. Geotechnique 15 (1), 79–93.

Nguyen, D.K., Nguyen, T.P., Keawsawasvong, S., Lai, V.Q., 2021. Vertical uplift capacity of circular anchors in clay by considering anisotropy and non-homogeneity. Transp. Infrastruct. Geotech. https://doi.org/10.1007/s40515-021-00191-6.

OptumCE, 2020. OptumG2. Optum Computational Engineering, Copenhagen, Denmark. https://optumce.com/. (Accessed 1 December 2020).

Qian, Z.G., Li, A.J., Merifield, R.S., Lyamin, A.V., 2015. Slope stability charts for two-layered purely cohesive soils based on finite-element limit analysis methods. Int. J. GeoMech. 15 (3), 06014022.

Qureshi, M.U., Mahmood, Z., Rasool, A.M., 2021. Using multivariate adaptive regression splines to develop relationship between rock quality designation and permeability. J. Rock Mech. Geotech. Eng. https://doi.org/10.1016/j.jrmge.2021.06.011.

Raghuvanshi, T.K., 2019. Plane failure in rock slopes–A review on stability analysis techniques. J. King Saud Univ. Sci. 31 (1), 101–109.

Raja, M.N.A., Shukla, S.K., 2021. Multivariate adaptive regression splines model for reinforced soil foundations. Geosynth. Int. 28 (4), 368–390.

Renani, H.R., Martin, C.D., 2020. Factor of safety of strain-softening slopes. J. Rock Mech. Geotech. Eng. 12 (3), 473–483.

Schlotfeldt, P., Elmo, D., Panton, B., 2018. Overhanging rock slope by design: an integrated approach using rock mass strength characterisation, large-scale numerical modelling and limit equilibrium methods. J. Rock Mech. Geotech. Eng. 10 (1), 72–90.

Shiau, J., Lyamin, A.V., Sloan, S.W., 2004. Rigorous solution of classical lateral earth pressures. In: Proceedings of the 6th Young Geotechnical Professionals Conference. Gold Coast, Australia, pp. 162–167.

Shiau, J., Lyamin, A.V., Sloan, S.W., 2006. Application of pseudo-static limit analysis in geotechnical earthquake design. In: Proceedings of the 6th European Conference on Numerical Methods in Geotechnical Engineering. Graz, Austria.
Shiau, Jim S., Watson, J.F., 2008. 3D bearing capacity of shallow foundations located near deep excavation sites. In: Proceedings of the 2008 International Conference on Deep Excavation: Challenges Risk Management of Underground Construction (ICDE 2008). Singapore.
Shiau, J., Watson, J.F., Arnold, M.D., 2008a. Numerical study of a shallow foundation located near 45 degree slopes. In: Proceedings of the 4th International Conference on Advances in Structural Engineering and Mechanics. Jeju, Korea.
Shiau, J., Watson, J.F., Smith, C.A., 2008b. Foundation located near slope: a FLAC study. In: Proceedings of the 1st International FLAC/DEM Symposium on Numerical Modeling. Minneapolis, USA.
Shiau, J.S., Merifield, R.S., Lyamin, A.V., Sloan, S.W., 2011. Undrained stability of footings on slopes. Int. J. GeoMech. 11 (5), 381–390.
Shiau, J., Al-Asadi, F., 2020a. Three-dimensional analysis of circular tunnel headings using Broms and Bennermarks' original stability number. Int. J. GeoMech. 20 (7), 06020015.
Shiau, J., Al-Asadi, F., 2020b. Three-dimensional heading stability of twin circular tunnels. Geotech. Geol. Eng. 38 (3), 2973–2988.
Shiau, J., Al-Asadi, F., 2021a. Twin tunnels stability factors f_c, f_s and f_γ. Geotech. Geol. Eng. 39 (1), 335–345.
Shiau, J., Al-Asadi, F., 2021b. Revisiting circular tunnel stability using broms and bennermarks' original stability number. Int. J. GeoMech. 21 (5).
Shiau, J., Al-Asadi, F., 2022. Stability factors fc, fs and fγ for twin tunnels in three dimensions. Int. J. GeoMech. https://doi.org/10.1061/(ASCE)GM.1943-5622.0002264.
Shiau, J., Keawsawasvong, S., Lee, J.S., 2022. Three-dimensional stability investigation of trapdoors in collapse and blowout conditions. Int. J. GeoMech. 22 (4), 04022007.
Siacara, A.T., Napa-García, G.F., Beck, A.T., Futai, M.M., 2020. Reliability analysis of earth dams using direct coupling. J. Rock Mech. Geotech. Eng. 12 (2), 366–380.
Sirimontree, S., Jearsiripongkul, T., Lai, V.Q., Eskandarinejad, A., Lawongkerd, J., Seehavong, S., Thongchom, C., Nuaklong, Peem, Keawsawasvong, S., 2022. Prediction of penetration resistance of a spherical penetrometer in clay using multivariate adaptive regression splines model. Sustainability 14 (6), 3222.
Steinberg, D., Colla, P.L., Martin, K. 1999. https://www.emc.ncep.noaa.gov/research/JointOSSEs/references/MarsUserGuide.pdf (Accessed 27 June 2022).
Taylor, D.W., 1937. Stability of earth slopes. J. Boston Soc. Civ. Eng. 24 (3), 197–246.
Taylor, D.W., 1948. Fundamentals of Soil Mechanics. John Wiley & Sons, New York, NY, USA.
Ukritchon, B., Keawsawasvong, S., 2017. Error in Ito and Matsui's limit equilibrium solution of lateral force on a row of stabilizing piles. J. Geotech. Geoenviron. Eng. 143 (9), 02817004.
Ukritchon, B., Keawsawasvong, S., 2018. A new design equation for drained stability of conical slopes in cohesive-frictional soils. J. Rock Mech. Geotech. Eng. 10 (2), 358–366.
Ukritchon, B., Keawsawasvong, S., 2019a. Lower bound solutions for undrained face stability of plane strain tunnel headings in anisotropic and non-homogeneous clays. Comput. Geotech. 112, 204–217.
Ukritchon, B., Keawsawasvong, S., 2019b. Three-dimensional lower bound finite element limit analysis of an anisotropic undrained strength criterion using second-order cone programming. Comput. Geotech. 106, 327–344.
Ukritchon, B., Keawsawasvong, S., 2019c. Stability of retained soils behind underground walls with an opening using lower bound limit analysis and second-order cone programming. Geotech. Geol. Eng. 37 (3), 1609–1625.
Ukritchon, B., Keawsawasvong, S., 2019d. Design equations of uplift capacity of circular piles in sands. Appl. Ocean Res. 90, 101844.
Ukritchon, B., Yoang, S., Keawsawasvong, S., 2019. Three-dimensional stability analysis of the collapse pressure on flexible pavements over rectangular trapdoors. Transportation Geotechnics 21, 100277.
Ukritchon, B., Keawsawasvong, S., 2020a. Undrained lower bound solutions for end bearing capacity of shallow circular piles in non-homogeneous and anisotropic clays. Int. J. Numer. Anal. Methods GeoMech. 44 (5), 596–632.
Ukritchon, B., Keawsawasvong, S., 2020b. Undrained stability of unlined square tunnels in clays with linearly increasing anisotropic shear strength. Geotech. Geol. Eng. 38 (1), 897–915.
Ukritchon, B., Yoang, S., Keawsawasvong, S., 2020. Undrained stability of unsupported rectangular excavations in non-homogeneous clays. Comput. Geotech. 117, 103281.
Wang, L., Wu, C., Gu, X., Liu, H., Mei, G., Zhang, W., 2020a. Probabilistic stability analysis of earth dam slope under transient seepage using multivariate adaptive regression splines. Bull. Eng. Geol. Environ. 79 (6), 2763–2775.
Wang, L., Wu, C., Tang, L., Zhang, W., Lacasse, S., Liu, H., Gao, L., 2020b. Efficient reliability analysis of earth dam slope stability using extreme gradient boosting method. Acta Geotechnica 15 (11), 3135–3150.
Wu, L., Fan, J., 2019. Comparison of neuron-based, kernel-based, tree-based and curve-based machine learning models for predicting daily reference evapotranspiration. PLoS One 14 (5), e0217520.
Xie, M., Wang, Z., Liu, X., Xu, B., 2011. Three-dimensional critical slip surface locating and slope stability assessment for lava lobe of Unzen volcano. J. Rock Mech. Geotech. Eng. 3 (1), 82–89.
Yang, G., Zhong, Z., Zhang, Y., Fu, X., 2015. Optimal design of anchor cables for slope reinforcement based on stress and displacement fields. J. Rock Mech. Geotech. Eng. 7 (4), 411–420.
Yang, Y., Wu, W., Zheng, H., 2020. Searching for critical slip surfaces of slopes using stress fields by numerical manifold method. J. Rock Mech. Geotech. Eng. 12 (6), 1313–1325.
Yang, X.L., Chen, H., 2021. Seismic analysis of 3D active earth pressure for unsaturated backfill. Transp. Geotech. 30, 100593.
Yodsomjai, W., Keawsawasvong, S., Senjuntichai, T., 2021a. Undrained stability of unsupported conical slopes in anisotropic clays based on AUS failure criterion. Transp. Infrastruct. Geotechno. 8, 557–568.
Yodsomjai, W., Keawsawasvong, S., Lai, V.Q., 2021b. Limit analysis solutions for bearing capacity of ring foundations on rocks using Hoek–Brown failure criterion. Int. J. Geosynth. Ground Eng. 7 (2), 1–10.
Yodsomjai, W., Lai, V.Q., Banyong, B., Chauhan, V.B., Thongchom, C., Keawsawasvong, S., 2022. A machine learning regression approach for predicting basal heave stability of braced excavation in non-homogeneous clay. Arabian J. Geosci. 15, 873.
Zhang, F., Liu, G., Chen, W., Liang, S., Chen, R., Han, W., 2012. Human-induced landslide on a high cut slope: a case of repeated failures due to multi-excavation. J. Rock Mech. Geotech. Eng. 4 (4), 367–374.
Zhang, W.G., Goh, A.T.C., 2013. Multivariate adaptive regression splines for analysis of geotechnical engineering systems. Comput. Geotech. 48, 82–95.
Zhang, W., 2019. MARS Applications in Geotechnical Engineering Systems. Springer jointly published with Science Press, Beijing, China, Beijing.
Zhang, W., Zhang, R., Wang, W., Zhang, F., Goh, A.T.C., 2019a. A Multivariate Adaptive Regression Splines model for determining horizontal wall deflection envelope for braced excavations in clays. Tunn. Undergr. Space Technol. 84, 461–471.
Zhang, W., Wu, C., Li, Y., Wang, L., Samui, P., 2019b. Assessment of pile drivability using random forest regression and multivariate adaptive regression splines. Georisk 114.
Zhang, W., Zhang, R., Wu, C., Goh, A.T.C., Lacasse, S., Liu, Z., Liu, H., 2020. State-of-the-art review of soft computing applications in underground excavations. Geosci. Front. 11 (4), 1095–1106.
Zhang, Z.L., Yang, X.L., 2021. Seismic stability analysis of slopes with cracks in unsaturated soils using pseudo-dynamic approach. Transp. Geotech. 29, 100583.
Zhang, W., Wu, C., Zhong, H., Li, Y., Wang, L., 2021. Prediction of undrained shear strength using extreme gradient boosting and random forest based on Bayesian optimization. Geosci. Front. 12 (1), 469–477.
Zhang, W., Li, H., Han, L., Chen, L., Wang, L., 2022. Slope stability prediction using ensemble learning techniques: a case study in Yunyang County, Chongqing, China. J. Rock Mech. Geotech. Eng. https://doi.org/10.1016/j.jrmge.2021.12.011.
Zheng, G., Yang, P., Zhou, H., Zeng, C., Yan, X., He, X., Yu, X., 2019. Evaluation of the earthquake induced uplift displacement of tunnels using multivariate adaptive regression splines. Comput. Geotech. 113, 103099.
Zhou, H., Xu, H., Yu, X., Guo, Z., Zheng, G., Yang, X., Tian, Y., 2021. Evaluation of the bending failure of columns under an embankment loading. Int. J. GeoMech. 21 (7), 04021112.

Jim Shiau is currently Associate Professor at University of Southern Queensland (USQ), Australia. He received the PhD from University of Newcastle, NSW, Australia where he continued two years of post-doctorate under the leadership of late Laureate Professor Scott Sloan. His research focuses on deep braced excavation and soft ground tunneling, sinkhole stability, finite element limit and shakedown analyses for geotechnical stability problems. Jim Shiau has extensive experience in the design of underground structures. He enjoys the breadth of general practice with interests in geotechnical stability research. He has published more than 15 articles in high-impact top 25% journal as the first and corresponding author. Jim Shiau has also involved in the organization of several international conferences in Australia since 2014. Jim Shiau is a passionate and creative educator in geotechnical engineering. He is experienced in geotechnical education with the uses of project-based learning, physical modeling, and short videos for online learning. He was a winner of the USQ Teaching Award.